Supplement of Atmos. Chem. Phys., 15, 7003–7015, 2015
http://www.atmos-chem-phys.net/15/7003/2015/
doi:10.5194/acp-15-7003-2015-supplement

Atmospheric Chemistry and Physics Open Access

Supplement of

Simulation of the isotopic composition of stratospheric water vapour – Part 2: Investigation of HDO / H_2O variations

R. Eichinger et al.

Correspondence to: R. Eichinger (roland.eichinger@dlr.de)

Supplement of

Simulation of the isotopic composition of stratospheric water vapour – Part 2: Investigation of HDO and H_2O variations

R. Eichinger[1], P. Jöckel[1], and S. Lossow[2]

[1] Deutsches Zentrum für Luft- und Raumfahrt
Institut für Physik der Atmosphäre
Oberpfaffenhofen, 82230 Wessling, Germany

[2] Karlsruhe Institute of Technology
Institute for Meteorology and Climate Research
Hermann-von-Helmholtz-Platz 1, 76344 Leopoldshafen, Germany

Roland.Eichinger@dlr.de

Supplementary material for our article "Simulation of the isotopic composition of stratospheric water vapour – Part 2: Investigation of HDO and H_2O variations" in Atmos. Chem. Phys. (2014), available at: http://www.atmos-chem-phys.net

Date: April 20, 2015

Contents

1 Introduction

This supplement provides additional information to the article "Simulation of the isotopic composition of stratospheric water vapour – Part 2: Investigation of HDO and H_2O variations".

2 Combination of the satellite time series

2.1 Satellite data sets

The combined satellite time series is based on observations of the HALOE and MIPAS instruments.

HALOE was an instrument on UARS (Upper Atmosphere Research Satellite) providing data from September 1991 to November 2005. It employed the solar occultation technique measuring the attenuation of solar radiance during 15 sunrises and 15 sunsets per day. Based on the viewing geometry and the UARS orbit a latitudinal coverage between roughly 60°S and 60°N could be achieved within a month, while over a year the coverage extended from 80°S to 80°S. Water vapour results were retrieved from spectral information in the wavelength range between 6.54 μm and 6.67 μm (1500 cm^{-1} – 1528 cm^{-1}), typically in the altitude range from 10 km up to about 85 km (Russell et al., 1993). Here data from the retrieval version 19 are used (e.g. Randel et al., 2006; Scherer et al., 2008).

The MIPAS instrument was deployed on Envisat (Environmental Satellite) performing observations from 2002 to 2012. Different than HALOE the instrument measured the thermal emission at the atmospheric limb providing more than 1000 observations per day. Envisat used a polar, sun-synchronous orbit that allowed a latitudinal coverage from pole to pole on a daily basis (Fischer et al., 2008). The MIPAS data set is split into two parts due to an instrument failure in 2004. From 2002 to March 2004 MIPAS measured with its nominal resolution of 0.035 cm $^{-1}$ (designated as full resolution period – FR). Measurement recommenced in 2005 however with a reduced resolution of 0.0625 cm^{-1} (reduced resolution period – RR). For the combined satellite time series MIPAS data retrieved with the IMK/IAA (Institut für Meteorologie und Klimaforschung in Karlsruhe, Germany / Instituto de Astrofísica de Andalucía" in Granada, Spain) processor are used, i.e. versions 20 (FR) and 220/221 (RR). For both periods the water vapour information is retrieved from a dozen of microwindows distributed over the wavelength range between 7.09 μm and 12.57 μm (795 cm $^{-1}$ – 1411 cm^{-1}) covering the altitude range from about 10 km to the lower mesosphere.

2.2 Combination of the satellite data sets

The combination of the satellite data sets requires a handling of the biases that exist among them (Milz et al., 2009). For that in a first step monthly zonal means of the individual data sets are derived. In a second step the MIPAS data are adjusted towards HALOE by a scalar, time independent shift S that minimises the offset between both data sets in the overlap period in a root mean square sense:

$$RMS = \sqrt{\frac{1}{n} \cdot \sum_{i=1}^{n} \left[x_{i,H} - (x_{i,M} + S)\right]^2} \tag{1}$$

Here $x_{i,H}$ and $x_{i,M}$ denote the individual overlapping data points for HALOE and MIPAS and n describes the their total number. The shift S_{opt} that minimises Eq. 1 is given by:

$$S_{opt} = \frac{1}{n} \cdot \sum_{i=1}^{n} (x_{i,H} - x_{i,M}) \tag{2}$$

In a last step the overlapping HALOE and shifted MIPAS data points are averaged using their associated standard errors w_i from the monthly and zonal mean derivation as weights.

$$x_i = \frac{w_{i,H} \cdot x_{i,H} + w_{i,M} \cdot (x_{i,M} + S_{opt})}{w_{i,H} + w_{i,M}} \tag{3}$$

Figure 1 shows an example for the latitude range between 10°S and 10°N at an altitude of 25 km. In the upper panel the monthly zonal mean time series of HALOE is shown by the black line. The original MIPAS time series are given in blue. Both, for the full and reduced resolution period, the MIPAS data show higher volume mixing ratios than HALOE, as expected from earlier assessments (e.g. Kley et al., 2000; Milz et al., 2009). This aspect has to be taken into account when comparing the combined time series to other data sets. The adjusted MIPAS time series are shown in green and the final combined time series is shown in red. The lower panel shows the root mean square of the offset between HALOE and MIPAS in the overlap periods as function of the MIPAS shift S according to Eq. 1. The optimal shift S_{opt} of the MIPAS time series is indicated by the dashed line. For the full resolution period (black) the optimal shift is 0.43 ppmv and for the reduced resolution (grey) it is 0.33 ppmv. Overall, the shifts for both MIPAS periods are very similar as function of altitude and latitude (not shown here).

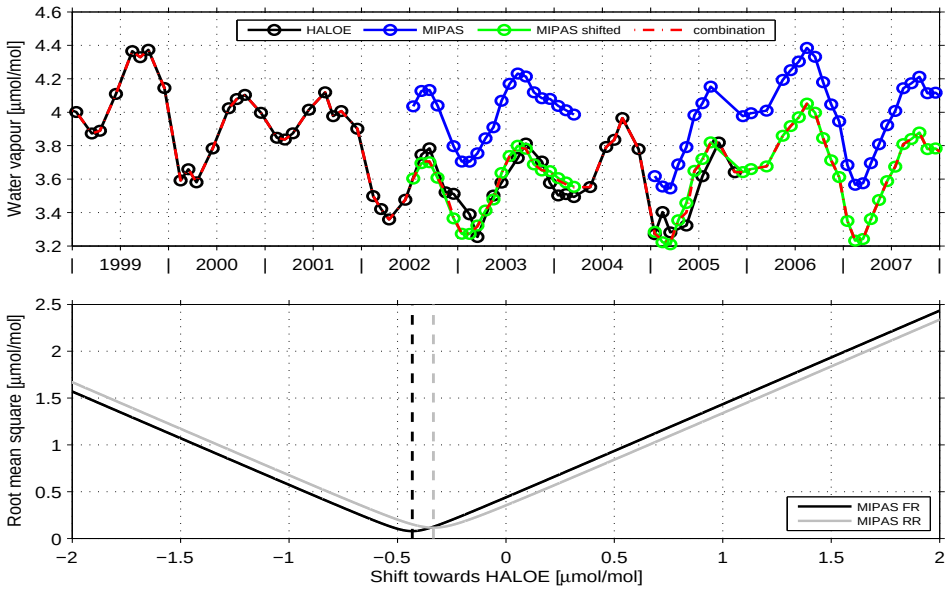

Figure 1: Example of the satellite data combination considering the zonal mean between 10°S – 10°N at 25 km. The upper panel shows the monthly mean HALOE and MIPAS time series in black and blue, respectively. The green line depicts the adjusted MIPAS time series and the combined time series is given by the red dash-dotted line. The lower panel shows the relationship between the shift of the MIPAS time series and the root mean square of the offset towards HALOE for the full (black) and reduced resolution period (grey) of MIPAS. The optimal shift of the MIPAS time series is indicated by the dashed lines.

3 Description of the modified chemical tendency of HDO

Here, we describe the modification of the additional EMAC simulation, applied for the investigation of the influence of methane isotope effects on the stratospheric δD(H_2O) tape recorder in Sect. 4. From the simulation described in Sect. 3, it differs in only one point: The calculation of the **c**hemical contribution to the tendency of HDO ($\frac{\partial(HDO)}{\partial t}|_C$) was implemented in a different manner. With the aim to suppress the influence of the chemistry on δD(H_2O), in a sensitivity simulation, the following approach was introduced:

$$\delta D'_a(H_2O) = \delta D_b(H_2O). \tag{4}$$

Here $\delta D'_{ac}(H_2O)$ represents the modified δD(H_2O) value **a**fter the addition of the chemical tendencies of HHO and HDO to their total tendencies and $\delta D_{bc}(H_2O)$ stands for δD(H_2O) **b**efore this operation. In order to fulfil this condition, a modified calculation of the chemical HDO tendeny was implemented into the H2OISO submodel. Considering the δ-notation

$$\delta D(H_2O) = \frac{R_{sample} - R_{VSMOW}}{R_{VSMOW}} \cdot 1000 = \left(\frac{R_{sample}}{R_{VSMOW}} - 1\right) \cdot 1000, \tag{5}$$

where R denotes the ratio of HDO to H_2O of the respective compound, Eq. 4 gives

$$\left[\frac{\left(\frac{HDO + \frac{\partial(HDO)}{\partial t}|_T \cdot \Delta t + \frac{\partial(HDO)}{\partial t}|_{C'} \cdot \Delta t}{HHO + \frac{\partial(HHO)}{\partial t}|_T \cdot \Delta t + \frac{\partial(HHO)}{\partial t}|_C \cdot \Delta t}\right)}{R_{VSMOW}} - 1\right] \cdot 1000 = \left[\frac{\left(\frac{HDO + \frac{\partial(HDO)}{\partial t}|_T \cdot \Delta t}{HHO + \frac{\partial(HHO)}{\partial t}|_T \cdot \Delta t}\right)}{R_{VSMOW}} - 1\right] \cdot 1000, \tag{6}$$

with $\frac{\partial(HDO)}{\partial t}|_T$ and $\frac{\partial(HHO)}{\partial t}|_T$ denoting the **t**otal tendencies before the addition of the chemical tendencies for the HDO and the HHO tracer, respectively. $\frac{\partial(HDO)}{\partial t}|_C$ stands for the chemical tendency of the HHO tracer and $\frac{\partial(HDO)}{\partial t}|_{C'}$ for the modified chemical tendency of the HDO tracer. HDO and HHO represent the $t-1$ values of the respective tracers and Δt the time step. Solving Eq. 6 for $\frac{\partial(HDO)}{\partial t}|_{C'} \cdot \Delta t$ leads to

$$\frac{\partial(HDO)}{\partial t}|_{C'} = \frac{\partial(HHO)}{\partial t}|_C \cdot \frac{HDO + \frac{\partial(HDO)}{\partial t}|_T \cdot \Delta t}{HHO + \frac{\partial(HHO)}{\partial t}|_T \cdot \Delta t} \tag{7}$$

for the modified chemical tendency of HDO. This modified chemical HDO tendency is always consistent with the chemical tendency of HHO, but δD(H_2O) does not become influenced by methane oxidation. In other words, in this sensitivity simulation, CH_4 and CH_3D have the same life times. This calculation can provide insight into the sensitivity of stratospheric δD(H_2O) patterns (e.g. the tape recorder) on the oxidation of CH_4 and CH_3D.

4 Additional images

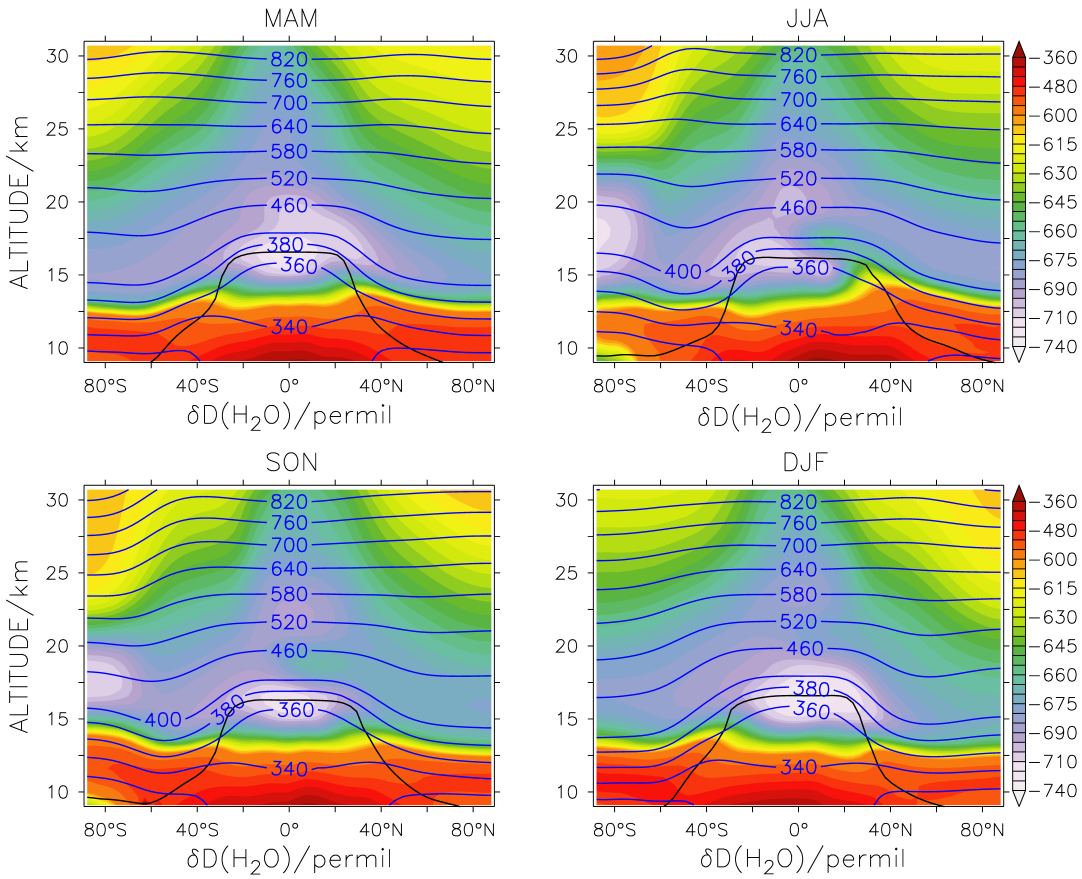

Figure 2: Zonally and seasonally averaged δD(H_2O) (coloured), tropopause height (black lines) and isentropes (blue contour lines) in K, averaged over the 21 years of the EMAC simulation. MAM: March, April, May; JJA: June, July, August; SON: September, October, November; DJF: December, January, February.

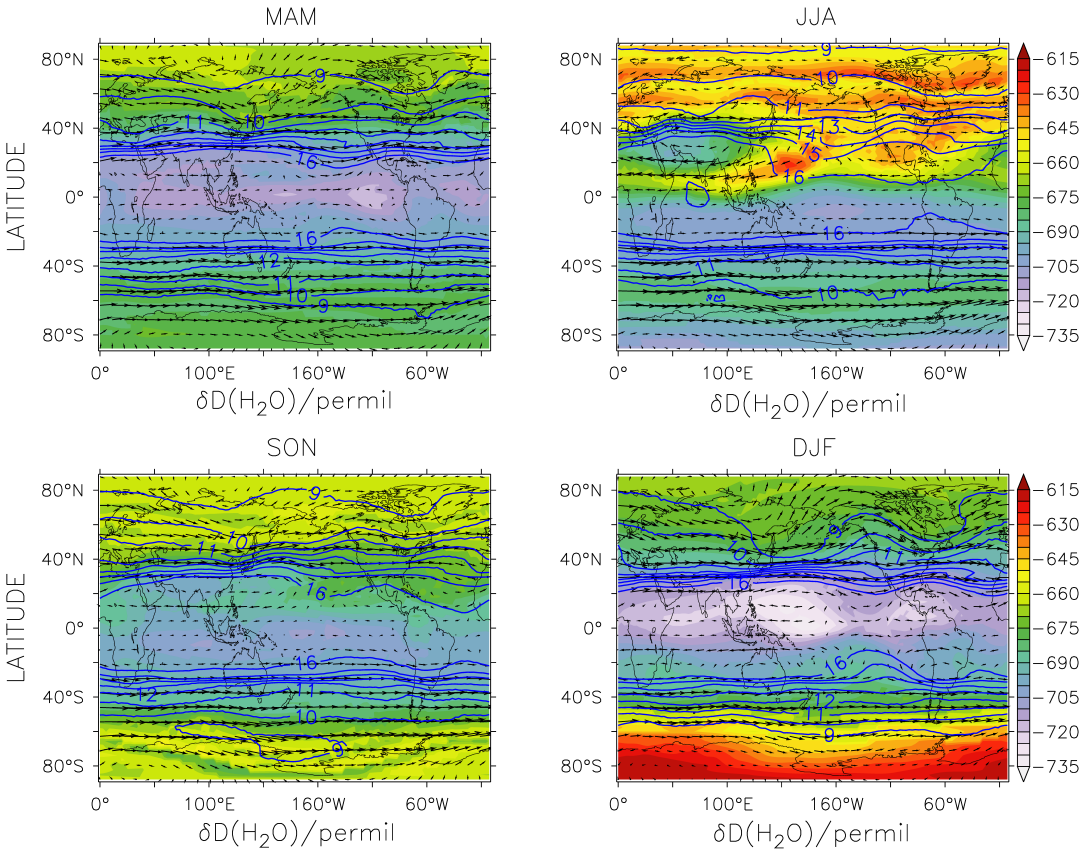

Figure 3: Seasonally averaged δD(H_2O) (colours), horizontal wind vectors (arrows) averaged from the 380 to the 400 K isentrope and the tropopause height (blue contour lines), averaged over the 21 years of the EMAC simulation. MAM: March, April, May; JJA: June, July, August; SON: September, October, November; DJF: December, January, February.

References

Fischer, H., Birk, M., Blom, C., Carli, B., Carlotti, M., von Clarmann, T., Delbouille, L., Dudhia, A., Ehhalt, D., Endemann, M., Flaud, J. M., Gessner, R., Kleinert, A., Koopman, R., Langen, J., López-Puertas, M., Mosner, P., Nett, H., Oelhaf, H., Perron, G., Remedios, J., Ridolfi, M., Stiller, G. P., and Zander, R.: MIPAS: An instrument for atmospheric and climate research, Atmospheric Chemistry & Physics, 8, 2151 – 2188, doi:10.5194/acp-8-2151-2008, 2008.

Kley, D., Russell, J. M., and Philips, C.: Stratospheric Processes and their Role in Climate (SPARC) - Assessment of upper tropospheric and stratospheric water vapour, SPARC Report 2, WMO/ICSU/IOC World Climate Research Programme, Geneva, 2000.

Milz, M., Clarmann, T. V., Bernath, P., Boone, C., Buehler, S. A., Chauhan, S., Deuber, B., Feist, D. G., Funke, B., Glatthor, N., Grabowski, U., Griesfeller, A., Haefele, A., Höpfner, M., Kämpfer, N., Kellmann, S., Linden, A., Müller, S., Nakajima, H., Oelhaf, H., Remsberg, E., Rohs, S., Russell, III, J. M., Schiller, C., Stiller, G. P., Sugita, T., Tanaka, T., Vömel, H., Walker, K., Wetzel, G., Yokota, T., Yushkov, V., and Zhang, G.: Validation of water vapour profiles (version 13) retrieved by the IMK/IAA scientific retrieval processor based on full resolution spectra measured by MIPAS on board Envisat, Atmospheric Measurement Techniques, 2, 379 – 399, 2009.

Randel, W. J., Wu, F., VöMel, H., Nedoluha, G. E., and Forster, P.: Decreases in stratospheric water vapor after 2001: Links to changes in the tropical tropopause and the Brewer-Dobson circulation, Journal of Geophysical Research, 111, D12 312, doi:10.1029/2005JD006744, 2006.

Russell, J. M., Gordley, L. L., Park, J. H., Drayson, S. R., Hesketh, W. D., Cicerone, R. J., Tuck, A. F., Frederick, J. E., Harries, J. E., and Crutzen, P. J.: The Halogen Occultation Experiment, Journal of Geophysical Research, 98, 10 777 – 10 797, 1993.

Scherer, M., Vömel, H., Fueglistaler, S., Oltmans, S. J., and Staehelin, J.: Trends and variability of mid-latitude stratospheric water vapour deduced from the re-evaluated Boulder balloon series and HALOE, Atmospheric Chemistry & Physics, 8, 1391 – 1402, doi:10.5194/acp-8-1391-2008, 2008.